Received: 7 October 2022 | Accepted: 3 November 2022

DOI: 10.1002/pamm.202200203

Objectivity and accuracy enhancement within ANN-based multiscale material modeling

Yousef Heider[1,*] and **WaiChing Sun**[2]

[1] Institute of General Mechanics, RWTH Aachen University. Eilfschornsteinstr. 18, 52062, Aachen, Germany

[2] Columbia University, Department of Civil Engineering and Engineering Mechanics, 614 SW Mudd, New York, NY 10027, USA

Nowadays, supervised machine learning (ML) via artificial neural network (ANN) is increasingly applied within multiscale material modeling and homogenization to generate data-based, physics-informed material models as an alternative to conventional material models. This application is associated with many benefits, such as increasing of computational efficiency and accuracy. However, the establishment of a reliable data-based or ML-based material model requires the availability of a proper and sufficiently large database from small-scale simulations and appropriate processing of these data as part of the model building steps. In this connection, this contribution discusses the method to generate ML-based material models, which strictly fulfill a number of restrictions, such as objectivity (or material frame-indifference) and thermodynamic consistency (second-law of thermodynamics) for an elasto-plastic material response. While focusing in this contribution on anisotropic crystal plasticity, the two aforementioned restrictions can be fulfilled via the utilization of informed-graph NN and the application of data representation in spectral form. The numerical results show that learning the ML model to explicitly predict the plastic strain as an intermediate step not only enhances the fulfillment of thermodynamic consistency but also improves the accuracy of the final prediction.

1 Introduction

In the literature, several publications show the efficiency of applying machine learning (ML) approaches, such as artificial neural networks (ANN), in multi-scale material modeling through computational homogenization of microscopically heterogeneous representative volume elements (RVEs). In this regard, applying "offline" ML multiscale modeling allows overcoming the disadvantages of computationally-expensive "online" multiscale homogenization methods or inaccurate phenomenological models. Moreover, it allows to include several microscopic information in the continuum mechanical framework, to discover new dependencies, and to waive the need to explicitly determine the material parameters. Of the first works in the domain of supervised machine learning for constitutive models count the paper of Ghaboussi et al. [1], applied to generate a stress-strain model for concrete under plane stress state. The proposed concepts were extended later by Lefik and Schrefler [2] to consider non-linear elasto-plastic hysteresis, where an incremental ANN form based on experimental data is considered. To mention some recent works, ANN multiscale model is proposed in [3] to capture the nonlinear elastic materials response. An implementation of supervised ANN in multi-scale multi-permeability poroplasticity can be found in [4]. In [5] and [6], ANN material models are developed to capture the structural response under nonlinear viscoplasticity and elasto-plasticity, respectively. In [7], ANN-based model that captures grain boundary constitutive behavior is proposed, whereas feed-forward NN within fracture mechanics is applied in [8].

The reliability and accuracy of the trained material model do not depend only on the size and quality of the database, but also on the form that data are represented in the training [9, 10], the flow of information in the model, and the NN settings and hyper-parameters [10–12]. Relying on the database acquired from the lower-scale anisotropic crystal plasticity simulations in Heider et al. [9], the objective of the underlying work is (1) to utilize a multi-step informed-graph-based neural network to enforce the fulfillment of the 2^{nd}-law of thermodynamics for the dissipative material response, and (2) enforce objectivity strictly by changing the representation of the stress and strain tensors from component to spectral form.

While the fulfillment of the objectivity and the entropy inequality assists in improving the accuracy and reliability of the developed ML material model, another factor that can contribute to the accuracy of the prediction is the proper choice of the hyperparameters of the neural networks. An automated way to discover the optimal NN settings, including model architecture, number of hidden layers, learning rate, activation function, epochs, batch size, and dropout rate, is presented in [11] in connection with ML-based permeability and retention curve models and in [10] in connection with elasto-plastic anisotropic composite materials. The basic idea is to apply deep reinforcement learning (DRL) to figure out the proper selection of the NN hyperparameters that are associated with a maximum pre-defined reward score (like prediction accuracy). The discussion of automated NN hyperparameter selection is, however, beyond the scope of this work.

The ML model in this work is implemented in Python deep learning open-source code Keras with Tensorflow as a backend package. The steps in building the ML anisotropic crystal plasticity can be briefly summarized as follows:

* Corresponding author: e-mail heider@iam.rwth-aachen.de, phone +49 241 80 98282

1. Data generation from lower-scale crystal plasticity simulations.
2. Applying spectral decomposition to compute the eigenvalues and eigenvector and, thus, the related Euler angles.
3. Splitting the data into input and output in addition to training, validation, and testing subsets.
4. Training the model after scaling (normalization) each sequence of data to be within the range [0, 1].
5. Testing the trained model on unseen data, where the predicted output can be rescaled to the original range using a similar scaling functionality.

To give an overview, the formation of an informed directed elasto-plastic graph (EPG), which enhances the thermodynamic consistency and objectivity, is presented in Section 2. This is followed by testing the accuracy and reliability of the proposed approach using a database related to anisotropic crystal plasticity in Section 3. This section includes also a comparison between the EPG approach and a simple incremental direct graph DG approach, which does not enhance thermodynamic consistency. Finally, concluding remarks and a future aspects are presented in Section 4.

2 Informed directed graph representation and objectivity enhancement

The focus of the following discussion is on generating a ML-based material model, which enhances the fulfillment of thermodynamic consistency and objectivity. For the generation of the database, the "ultimate algorithm" is applied according to [13], which delivers the exact solution of f.c.c. single-crystal plasticity within the small-strain framework. In addition to having the total strain $\boldsymbol{\varepsilon}$ as an input and the total stress $\boldsymbol{\sigma}$ as the final output, the intermediate steps in this algorithm deliver also important information, such as the plastic strain $\boldsymbol{\varepsilon}^p$, which can be used in the ML-model generation. For the thermodynamic consistency of the isothermal, elasto-plastic process, the rate of mechanical dissipation $\mathbb{D}_p$ must be non-negative. A common procedure in deriving an expression for $\mathbb{D}_p$ is to start with the Clausius-Duhem dissipation inequality, which is simplified to the local Clausius-Planck dissipation inequality for the purely mechanical and isothermal process. Following, e.g., [13–15], this can be expressed in terms of the stress power per unit volume $\boldsymbol{\sigma} \cdot \dot{\boldsymbol{\varepsilon}}$ and the rate of change of internal energy per unit volume $\dot{\Psi}$ as

$$\mathbb{D}_{loc} = \boldsymbol{\sigma} \cdot \dot{\boldsymbol{\varepsilon}} - \dot{\Psi} \geq 0\,. \tag{1}$$

For the elasto-plastic process under consideration, both $\boldsymbol{\varepsilon}$ and Ψ can be split into an elastic and a plastic contribution as $\boldsymbol{\varepsilon} = \boldsymbol{\varepsilon}^e + \boldsymbol{\varepsilon}^p$ and $\Psi = \Psi_{\text{el}}(\boldsymbol{\varepsilon}^e) + \Psi_{\text{pl}}(\boldsymbol{\varepsilon}^p)$, respectively. The time derivative of $\boldsymbol{\varepsilon}$ and Ψ read

$$\dot{\boldsymbol{\varepsilon}} = \dot{\boldsymbol{\varepsilon}}^e + \dot{\boldsymbol{\varepsilon}}^p \quad \text{and} \quad \dot{\Psi} = \dot{\Psi}_{\text{el}}(\boldsymbol{\varepsilon}^e) + \dot{\Psi}_{\text{pl}}(\boldsymbol{\varepsilon}^p) = \frac{\partial \Psi_{\text{el}}}{\partial \boldsymbol{\varepsilon}^e} \cdot \dot{\boldsymbol{\varepsilon}}^e + \dot{\Psi}_{\text{pl}}\,. \tag{2}$$

Inserting the terms of Eq. (2) in the inequality (1) yields

$$\mathbb{D}_{loc} = \left(\boldsymbol{\sigma} - \frac{\partial \Psi_{\text{el}}}{\partial \boldsymbol{\varepsilon}^e}\right) \cdot \dot{\boldsymbol{\varepsilon}}^e + \boldsymbol{\sigma} \cdot \dot{\boldsymbol{\varepsilon}}^p - \dot{\Psi}_{\text{pl}} \geq 0 \quad \longrightarrow \quad \mathbb{D}_p := \boldsymbol{\sigma} \cdot \dot{\boldsymbol{\varepsilon}}^p - \dot{\Psi}_{\text{pl}} \geq 0\,. \tag{3}$$

In this, the fulfillment of the entropy inequality for random positive or negative values of $\dot{\boldsymbol{\varepsilon}}^e$ requires $\boldsymbol{\sigma} = \dfrac{\partial \Psi_{\text{el}}}{\partial \boldsymbol{\varepsilon}^e}$. In order to enhance the fulfillment of the $\mathbb{D}_p \geq 0$ restriction, we propose an informed graph ML model for elasto-plasticity (EPG), illustrated in Fig. 1, that explicitly predicts the plastic strain in addition to the total stress. Additionally, we compare the performance of EPG with that of a simpler incremental direct graph DG, discussed in detail in [9], and does not explicitly include a prediction of the plastic strain.

The graphs in Fig. 1 represent incremental algorithms, where the information from the previous time step is used in the prediction of the variable at the next time step. They also include recurrent neural networks (RNN) for path-dependent plasticity and feed-forward regression neural networks (FFNN) for path-independent elasticity. Unlike DG, which is carried out in one step, the approach with EPG involves the following three steps:

1. RNN model to predict $\boldsymbol{\varepsilon}^p_{n+1}$ (plasticity)
2. Exact computation: $\boldsymbol{\varepsilon}^e_{n+1} = \boldsymbol{\varepsilon}_{n+1} - \boldsymbol{\varepsilon}^p_{n+1}$
3. FFNN model to predict $\boldsymbol{\sigma}_{n+1}$ based on $\boldsymbol{\varepsilon}^e_{n+1}$ (elasticity)

It is worth mentioning here that the RNN approach that is applied in this work is the Long Short-Term Memory (LSTM) neural network, introduced by Hochreiter and Schmidhuber [16].

ML material models should also follow the principle of material frame-indifference, i.e. should be objective or observer-invariance. Thus, in analogy to [9], the focus becomes in the ML model on the accurate prediction of both the eigenvalues and the direction of the eigenvectors, measured using, e.g. the corresponding Euler angles or the components of the

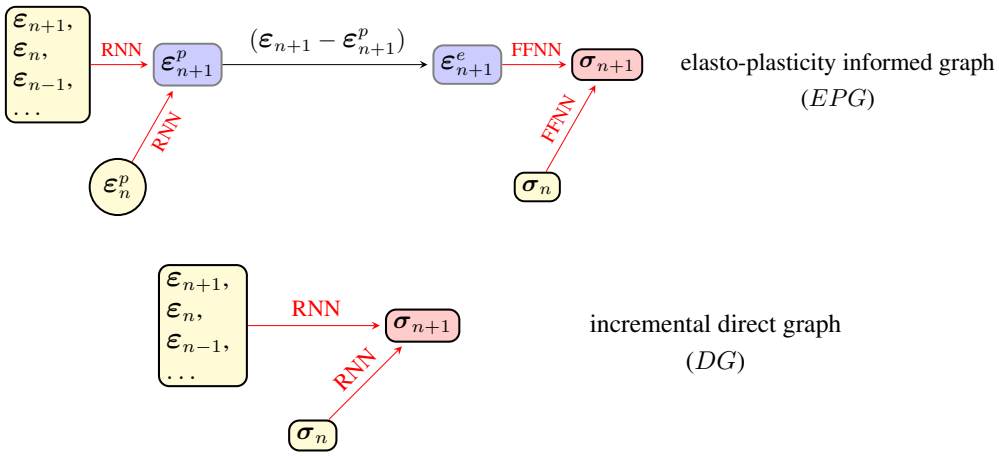

Fig. 1: Informed directed elasto-plastic graph (EPG) and incremental direct graph (DG), which show two methods for the information flow in the ML-based crystal plasticity material model. The yellow nodes represent the root nodes, the pink nodes are the target nodes, whereas the blue nodes are the intermediate nodes. The black arrow represents a definition and the red arrows represent the machine learning models, which are either recurrent neural networks (RNN) or feed-forward regression neural networks (FFNN)

skew-symmetric rotations in Lie Algebra. Therefore, a spectral decomposition is applied to compute the eigenvalues and eigenvectors of the total strain, plastic strain, and stress tensors as

$$\boldsymbol{\varepsilon} = \sum_{i=1}^{3} \varepsilon_i \left(\mathbf{n}_{\varepsilon i} \otimes \mathbf{n}_{\varepsilon i}\right) \quad , \quad \boldsymbol{\varepsilon}^p = \sum_{i=1}^{3} \varepsilon^p_i \left(\mathbf{n}_{\varepsilon^p i} \otimes \mathbf{n}_{\varepsilon^p i}\right) \quad , \quad \boldsymbol{\sigma} = \sum_{i=1}^{3} \sigma_i \left(\mathbf{n}_{\sigma i} \otimes \mathbf{n}_{\sigma i}\right), \tag{4}$$

where ε_i, ε^p_i, σ_i are the eigenvalues and $\mathbf{n}_{\varepsilon i}$, $\mathbf{n}_{\varepsilon^p i}$, $\mathbf{n}_{\sigma i}$ are the corresponding eigenvectors. The orthogonal and normalized eigenvectors allow to construct the (3×3) rotation tensors, for which the three Euler angles can be computed. The rotation tensors can be expressed as

$$\mathbf{R}_{\varepsilon} = \begin{bmatrix} \mathbf{n}_{\varepsilon 1} & \mathbf{n}_{\varepsilon 2} & \mathbf{n}_{\varepsilon 3} \end{bmatrix} \quad , \quad \mathbf{R}_{\varepsilon^p} = \begin{bmatrix} \mathbf{n}_{\varepsilon^p 1} & \mathbf{n}_{\varepsilon^p 2} & \mathbf{n}_{\varepsilon^p 3} \end{bmatrix} \quad , \quad \mathbf{R}_{\sigma} = \begin{bmatrix} \mathbf{n}_{\sigma 1} & \mathbf{n}_{\sigma 2} & \mathbf{n}_{\sigma 3} \end{bmatrix}, \tag{5}$$

where $\mathbf{R}_{\varepsilon}, \mathbf{R}_{\varepsilon^p}, \mathbf{R}_{\sigma} \in SO(3)$. Thus, the aim in the training of the ML model becomes, in addition to minimizing the discrepancy between the true and predicted eigenvalues, to minimize the distance between the true and the predicted rotation tensors, i.e between $\mathbf{R}_{\varepsilon^p}$ and $\mathbf{R}^M_{\varepsilon^p}$ for the plasticity step and between $\mathbf{R}_{\sigma}$ and $\mathbf{R}^M_{\sigma}$ for the elasticity step. To simplify the treatment, each rotation tensor with 9 components can be expressed by equivalent 3 quantities, which are in this work the Euler Angles. In particular, if we consider $\mathbf{R}_{\sigma}$ and $\mathbf{R}^M_{\sigma}$ as example, the true Euler angles can be expressed as $\{\overline{\varphi}_{\sigma}, \overline{\theta}_{\sigma}, \overline{\psi}_{\sigma}\} \in \mathbb{E} \subset \mathbb{R}^+$, whereas the predicted ones are $\{\overline{\varphi}^M_{\sigma}, \overline{\theta}^M_{\sigma}, \overline{\psi}^M_{\sigma}\} \in \mathbb{E} \subset \mathbb{R}^+$. With this, the *Euclidean distance* d between these angles can be computed and integrated in the loss function. This can be expressed for a certain test k as

$$\overline{\Phi}_k = \sqrt{d(\overline{\varphi}_{\sigma}, \overline{\varphi}^M_{\sigma})^2 + d(\overline{\theta}_{\sigma}, \overline{\theta}^M_{\sigma})^2 + d(\overline{\psi}_{\sigma}, \overline{\psi}^M_{\sigma})^2}\,. \tag{6}$$

With this, the total loss function $\mathcal{D}^{ML}_{\sigma R}$ can be expressed as the sum of the eigenvalue-related loss function $\mathcal{D}^{ML}_{\sigma}$ and eigenvector-related loss function $\mathcal{D}^{ML}_{R}$ as

$$\mathcal{D}^{ML}_{\sigma R} = \tfrac{1}{2}(\mathcal{D}^{ML}_{\sigma} + \mathcal{D}^{ML}_{R}) \quad \text{with} \quad \mathcal{D}^{ML}_{\sigma} = \frac{1}{N}\sum_{i=1}^{N}\left[\sigma_i - \overline{\sigma}^M_i\right]^2, \quad \text{and} \quad \mathcal{D}^{ML}_{R} = \frac{1}{N}\sum_{i=1}^{N}\overline{\Phi}_i\,, \tag{7}$$

where N is the number of output data points and $\overline{\sigma}^M_i$ are the predicted output data related to the eigenvalues of stress measure. In connection with the application of the Euclidean distance between the Euler angles for the loss function in the training, a non-uniqueness might be encountered under certain limit cases. For instance, $(\pi, \pi, 0)$ and $(0, 0, \pi)$ can represent the same rotation, however, their metric is not zero [17]. As a remedy to resolve this challenge is to impose the Euler angles to be in half-open ranges as $\varphi_i, \theta_i \in [-\pi, \pi)$ and $\psi_i \in [-\pi/2, \pi/2)$, which allows ϕ_{Eu} to be valid as a metric in the Special Orthogonal Group ($SO(3)$). Alternatively, different metrics can be applied, such as the "distance from the identity matrix" or the "geodesic on the unit sphere" in Lie algebra. A thoroughly discussion of different metrics can be found in [9], which is beyond the scope of this work.

3 Results and discussion

The aim of the following numerical experiments is to test the performance and show the accuracy and sources of error of the proposed informed elasto-plastic graph (EPG) in predicting the stress components in enhanced objectivity and thermodynamic consistency framework. Another aim is to compare EPG approach with the simpler DG with regard to the accuracy in predicting the stress components.

The dataset used in the generation of the ML material model consists of 1176 experiments, which result from 24 loading scenarios of the f.c.c crystal and for 49 states of rotation [9]. Within a plane-strain state, the crystal is subjected in each experiment to monotonic 100 increments of one or more strain components. These experiments are then split into a training subset (792), a validation subset (192), and a testing subset (192). Specifically, the **training subset** is used to adjust the neural network weights and biases, the **validation subset** is used in the training to regularly assess the quality of the trained model and thus contributes to the tuning of the NN weights, and the **testing subset** represents the unseen dataset and is employed for the final assessment of the trained ML model accuracy.

Fig. 2 illustrates the mean squared error (MSE) for each experiment of the training, validation, and testing datasets related to the RNN model to predict $\boldsymbol{\varepsilon}^p$ in the EPG approach. Specifically, Fig. 2, left, shows the overall MSE of the principal plastic strains and the corresponding Euler angles, whereas Fig. 2, middle and right, show, respectively, the MSE related only to the principal plastic strains and that corresponding to Euler angles. Apparently, the main source of errors is in the prediction of the rotation-related Euler angles. In this, few of the experiments show errors up to 4%, whereas most of the experiments show errors below 1%.

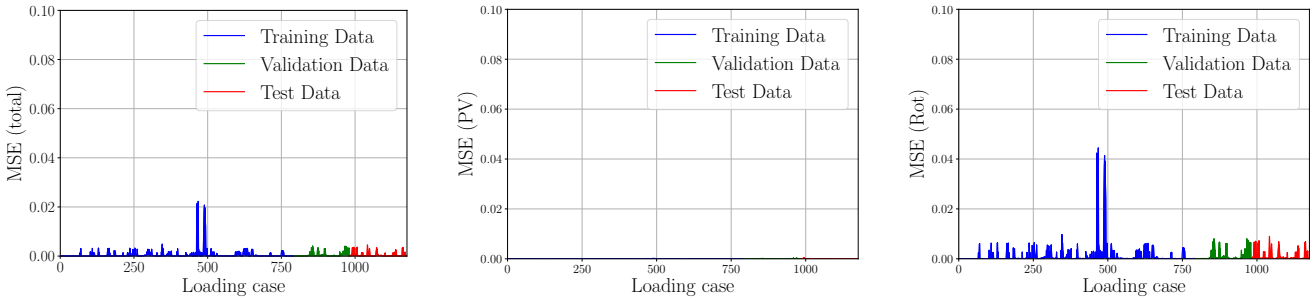

Fig. 2: Mean squared error (MSE) of the training, validation, and testing datasets related to the **RNN step to predict $\boldsymbol{\varepsilon}^p$** in the EPG approach. Overall MSE of the predicted principal plastic strains and the corresponding Euler angles (left), MSE related only to the principal plastic strains (middle), and MSE related only to the related Euler angles (right). The MSE of the principal plastic strains (middle figure) are too small in comparison with that of the Euler angles and, thus, barely visible as we fixed the MSE range for the three cases

In analogy, Fig. 3 illustrates the MSE for each experiment of the training, validation, and testing datasets related to the elastic step of the EPG approach with the FFNN step to predict $\boldsymbol{\sigma}$. Specifically, Fig. 3, left, shows the overall MSE of the principal stresses and the corresponding Euler angles, whereas Fig. 3, middle and right, show, respectively, the MSE related only to the principal stresses and that corresponding to Euler angles. As the elastic strain (input) in this step is computed based on the predicted strain from the plastic step, the main source of errors remains in the prediction of the rotation-related Euler angles. In this, few experiments show errors up to 5%, whereas most of the experiments show errors below or around 1%.

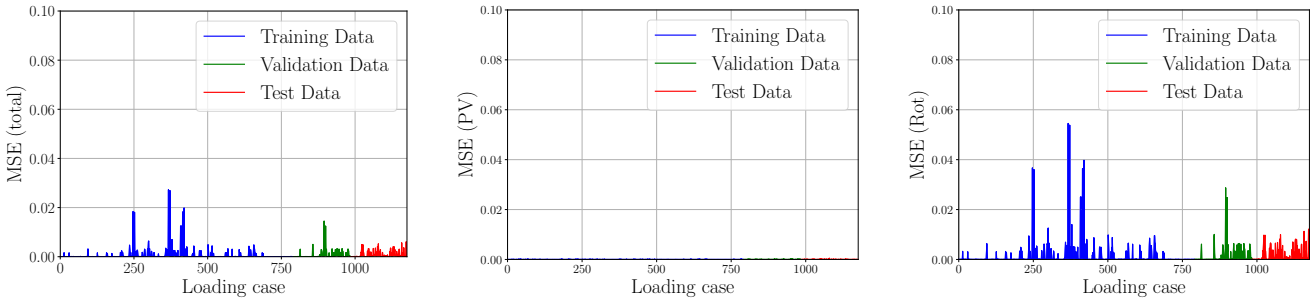

Fig. 3: Mean squared error (MSE) of the training, validation, and testing datasets related to the **FFNN step to predict $\boldsymbol{\sigma}$** in the EPG approach. Overall MSE of the predicted principal stresses and the corresponding Euler angles (left), MSE related only to the principal stresses (middle), and MSE related only to the Euler angles (right). The MSE of the principal plastic strains (middle figure) are too small in comparison with that of the Euler angles and, thus, barely visible as we fixed the MSE range for the three cases

For evaluating the performance of the ML model in a systematic way, we qualitatively compare between the MSE of the testing, validation, and training datasets based on calculating the non-parametric, empirical cumulative distribution functions (eCDFs), see, [18]. In particular, eCDFs are calculated for the MSE_i of testing (N_{testdata}), validation (N_{valddata}), and training ($N_{\text{traindata}}$) datasets considering all the components of plastic strain and stress (all), i.e. $i \in [1, N^{\text{all}}_{\text{testdata}}]$, $i \in [1, N^{\text{all}}_{\text{valddata}}]$, $i \in [1, N^{\text{all}}_{\text{traindata}}]$. Thus, for a dataset N with MSE_i sorted in ascending order, the eCDF can computed as

$$F_N(\text{MSE}) = \begin{cases} 0, & \text{MSE} < \text{MSE}_1, \\ \dfrac{r}{N}, & \text{MSE}_r \leq \text{MSE} < \text{MSE}_{r+1},\ r = 1, ..., N-1, \\ 1, & \text{MSE}_N \leq \text{MSE}\,. \end{cases} \tag{8}$$

Looking at the errors in Fig. 4 for both the plastic and elastic steps of the EPG approach, it is clear that the trained model does not suffer from over-fitting, i.e. the errors in the training subset are less than that of the testing subset. In the eCDF representation of the error, the more the curve is vertical, the better is the trained model as the error in all experiments becomes comparable. In this regard, Fig. 4, right, related for the final stress prediction, shows that the error in the unseen testing dataset is in the range $[10^{-5},\ 5 \times 10^{-3}]$, which reflects a good quality model.

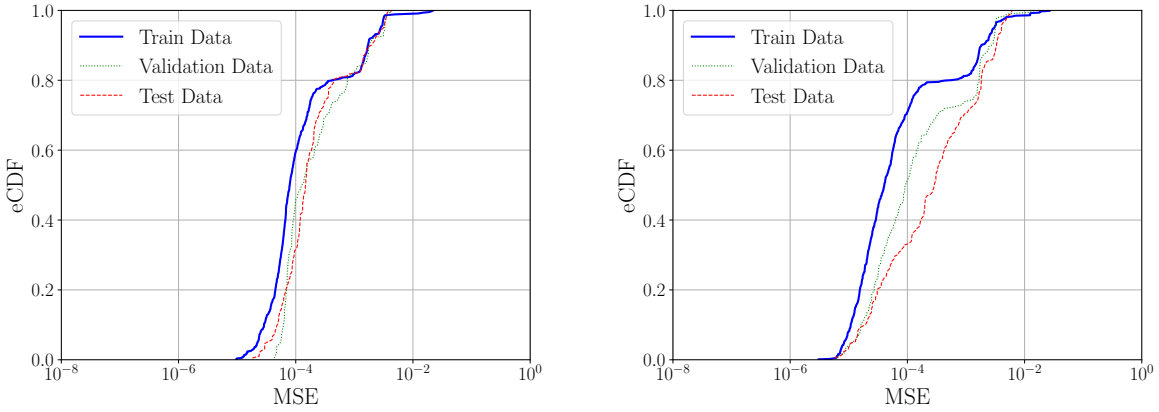

Fig. 4: eCDF vs. MSE of the training, validation, and testing datasets for the **RNN step to predict $\boldsymbol{\varepsilon}^p$** (left) and for the **FFNN step to predict $\boldsymbol{\sigma}$** (right) of the EPG approach

A quantitative comparison of the MSE between the elasto-plasticity informed graph (EPG) with enhanced objectivity and thermodynamic consistency and the incremental direct graph (DG) with merely enhance objectivity (see, [9]) is presented in Fig. 5. EPG outperforms DG for both MSE related to the principal stress values (PV) and the rotation-related quantities (Rot) of the testing dataset. This is particularly clear for the rotation-related quantities, where the eCDF - MSE curve is less steep.

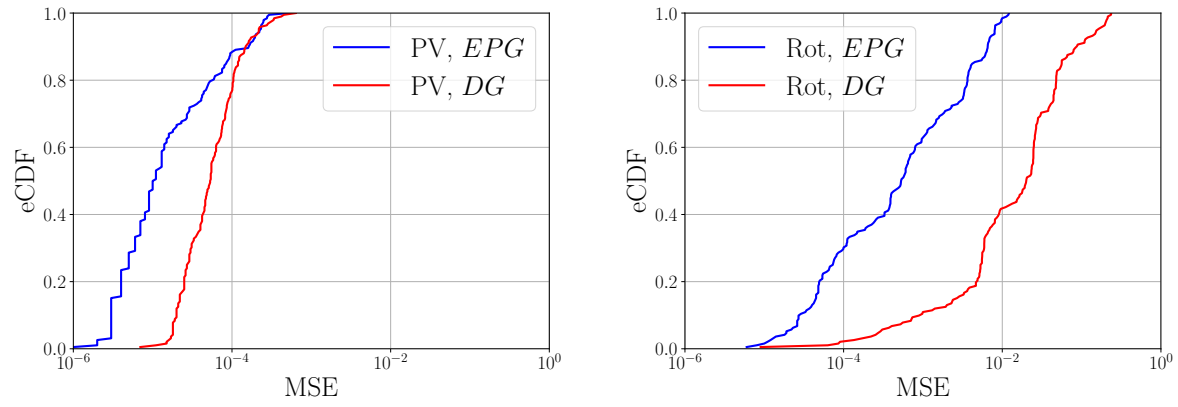

Fig. 5: eCDF vs. MSE related to the principal stress values (PV) and the rotation-related quantities (Rot) of the testing datasets using the EPG and DG approaches

4 Conclusions and future aspects

Within supervised machine learning, the underlying work aimed at generating a ML constitutive model of anisotropic, inelastic material, where both thermodynamic consistency and objectivity are enhanced. For this, an elasto-plastic, incremental informed-graph NN (EPG) is proposed, which is trained to predict the plastic strain and to predict the total stress that are parts of the dissipation inequality. Additionally, data representation in spectral form using Euler angles is applied to enhance the objectivity. In the numerical test cases, we examined the performance of the proposed EPG approach and we compared this to the simpler DG approach, where the thermodynamic consistency is not enhanced. The results showed that in all cases, the main source of errors is the prediction of the rotations. The comparisons showed also that EPG outperforms DG in the accuracy of prediction of both the principal stresses and the rotation-related quantities.

For future works, it is planned to extend this dataset to the geometric nonlinear regime and to incorporate the model in the finite element framework to replace the conventional material model in solving boundary-value-problems of crystal plasticity.

Acknowledgements This work relies on the dataset, related to the paper [9] and generated during the first author's work at the group of Professor WaiChing Sun, Columbia University (NYC), USA. Open access funding enabled and organized by Projekt DEAL.

References

[1] Ghaboussi J., Garrett Jr J., Wu X. (1991) Knowledge-based modeling of material behavior with neural networks. Journal of Engineering Mechanics. 117:132-153.
[2] Lefik M., Schrefler B. (2003) Artificial neural network as an incremental non-linear constitutive model for a finite element code. Comput. Methods Appl. Mech. Engrg. 192:3265-3283.
[3] Le B.A., Yvonnet J., He Q.-C. (2015) Computational homogenization of nonlinear elastic materials using neural networks. Int J Numer Methods Eng. 104:1061-1084.
[4] Wang K., Sun W.C. (2018) A multiscale multi-permeability poroplasticity model linked by recursive homogenizations and deep learning. Comput. Methods Appl. Mech. Eng. 334:337-380.
[5] Koeppe A., Bamer F., Markert B. (2019) Neural network based constitutive modeling of nonlinear viscoplastic structural response. Mech. Res. Commun. 95:85-88.
[6] Stoffel M., Bamer F., Markert B. (2019) An efficient Monte Carlo strategy for elasto-plastic structures based on recurrent neural networks. Acta Mechanica. 230:3279-3293.
[7] Fernandez M., Rezaei S., Mianroodi J.R., Fritzen F., Reese S. (2020) Application of artificial neural networks for the prediction of interface mechanics: a study on grain boundary constitutive behavior. AMSES. 7:1-27.
[8] Aldakheel F., Satari R., Wriggers P. (2021) Feed-Forward Neural Networks for Failure Mechanics Problems. Applied Sciences 11(14), DOI: 10.3390/app11146483.
[9] Heider Y., Wang K., Sun W.C. (2021) SO(3)-invariance of informed-graph-based deep neural network for anisotropic elastoplastic materials. Comput. Methods Appl. Mech. Engrg. 363:112875.
[10] Fuchs A., Heider Y., Wang K., Sun W.C., Kaliske M. (2021) DNN2: A hyper-parameter reinforcement learning game for self-design of neural network based elasto-plastic constitutive descriptions. Computers & Structures 249:106505.
[11] Heider Y., Suh H.S., Sun W.C. (2021) An offline multi-scale unsaturated poromechanics model enabled by self-designed/self-improved neural networks. Int J Numer Anal Methods Geomech 45(9):1212-1237.
[12] Heider Y. (2021) Multi-field and multi-scale computational fracture mechanics and machine-learning material modeling. Habilitation, Report No. IAM-13, RWTH Aachen University. DOI:10.18154/RWTH-2021-10362.
[13] Borja R.I. (2013) Plasticity: Modeling & Computation. Springer Science & Business Media. DOI:10.1007/978-3-642-38547-6.
[14] Yang H., Sinha S.K., Feng Y., McCallen D.B., Jeremić, B. (2018) Energy dissipation analysis of elastic–plastic materials. Comput. Methods Appl. Mech. Engrg. 331:309-326.
[15] Ali B., Heider Y., Markert B. (2022) Residual stresses in gas tungsten arc welding: a novel phase-field thermo-elastoplasticity modeling and parameter treatment framework. Comput Mech. 69:565-587.
[16] Hochreiter S., Schmidhuber J. (1997) Long short-term memory. Neural Comput. 9(8):1735-1780.
[17] Huynh D.Q. (2009) Metrics for 3D rotations: Comparison and analysis. J. Math. Imaging Vision 35(2):155-164.
[18] Gentle J.E. (2009) Computational Statistics. Springer, ISBN: 978-0-387-98145-1.

